

# Image Reconstruction from Multiple Frames of Sparse Data

R. RAMASESHAN AND B. YEGNANARAYANA

*Speech & Vision Laboratory, Department of Computer Science and Engineering, Indian Institute of Technology, Madras—600 036, India*

*Received March 27, 1992, Revised July 21, 1992, September 18, 1992*

**Abstract.** High-resolution image reconstruction from sparse data is an important problem in sensor array imaging (SAI). The reconstructed images from such a data are poorly resolved. However, there may exist possibilities of making multiple measurements, for example, collecting many frames of data in a dynamic scene situation where there is relative motion between the object and the receiver. We discuss here a method of reconstructing good-quality images from multiple frames of sparse data obtained from a simulated dynamic scene situation. This method, based on projection onto convex sets (POCS), not only restricts the solution set by satisfying the constraints in the multiple measurements but also reconstructs a high-resolution image.

**Key Words:** image reconstruction, sparse data, ill-posed problems, regularization, projection onto convex sets, sensor array imaging

## 1. Introduction

Image reconstruction is generally defined as a problem of estimating a two-dimensional image of an unknown object from its degraded data. The observations resulting from the reflected wave field from the object of interest are usually defined on a two-dimensional (2-D) real space  $\mathbf{R}^2$  or a two-dimensional complex space  $\mathbf{C}^2$ . The image formation is formulated by the linear model

$$g = h * f, \quad (\text{noise-free model}) \quad (1)$$

where  $g$  is obtained by the 2-D convolution ( $*$ ) of  $f$  with  $h$ . The image reconstruction is the process of obtaining the best estimate of  $f$ , given the observation  $g$ , and is known as the inverse problem. The observation  $g$  is usually degraded due to the image formation mechanism, or due to the recording medium or both. Due to degradations in the observed data, the solution to the inverse problem is not unique. The problem is ill-posed when the data is available only at a few points. In such a case (1) has many solutions since there are fewer equations than unknowns (underdetermined case).

The ill-posed problem has been studied extensively and a wide variety of solution methods are available to solve this problem [1–3]. Most of these methods have been unified under the theory of regularization of ill-posed problems ([4]). The basic idea in regularization is to restrict the space of acceptable solutions by choosing a function that minimizes an appropriate functional. Deterministic constraints can be used to reduce the solution space.

Constraints like finite support, nonnegativity or bounded energy, can be used as the a priori information in the reconstruction method. The method of projections onto convex sets (POCS) is useful when the constraints about the solution is known a priori. This method enables any number of a priori convex-type constraints to be incorporated in the algorithm, and it guarantees a weak convergence, i.e., inner product convergence [5]. Apart from restricting the solution space, it is also required to reconstruct a good-quality image from the observed data.

Several methods have been proposed to reconstruct a good-quality image from sparse data [6, 7]. The sparse data was collected for different frequencies of the wave illuminating the object. Through simulation studies, it was shown that the quality of the reconstructed image improved when sparse data collected from various frequencies were combined in the reconstruction algorithm. The image reconstruction algorithm was based on the method of POCS.

Another approach for reconstructing a good-quality image was proposed [8]. In this approach, the sparse data was collected by varying the object-receiver distance in a simulated sensor array imaging (SAI) setup. In this approach, it was shown that the quality of the reconstructed image improved as the data collected at various object-receiver distances were combined in the reconstruction algorithm. Another method for data collection using the variation of both frequency and object-receiver distance was also suggested. In these methods, multiple frames of data were collected when the object remained stationary throughout the imaging process.

A recursive procedure, based on weighted least-square theory for reconstructing a high-resolution image from a set of low-resolution noisy images was proposed [9]. Each image in the set had been shifted by a known amount with respect to a reference frame. The restoration procedure was carried out in the transform domain by first estimating the  $n$ th frame from the  $(n - 1)$ th frame, and then the actual measurements of the  $n$ th frame were incorporated to obtain a new estimate for the  $n$ th frame. They had shown that the image quality also improved as the number of frames were increased.

In this paper we propose a method based on POCS for image reconstruction from multiple frames of data obtained from a dynamic scene situation. The data collected from a dynamic scene not only contains the information regarding the image but also the information regarding the motion of the object. The objective here is to use all the information obtained from the multiple frames of data for image reconstruction. The motion parameters (shift values between one frame to the other) are assumed to be known. Preliminary results of reconstructing a good-quality image from multiple frames of sparse data were already reported [10]. The major differences between our approach and the approach proposed by Kim et al. [9] are (i) a method based on POCS is used to reconstruct an image from a sequence of sparse data frames; (ii) any arbitrary shift values can be used in the reconstruction algorithm; (iii) the shifts are incorporated in the spatial domain; (iv) the reconstruction is done by assuming a noiseless measurement of data; and (v) the data collection is done using a simulated SAI setup.

A brief review of the method of POCS is presented in Section 2. The basic SAI setup and the problems associated with it are discussed in Section 3. In Section-4, we show how the sparse nature of the data affects the solution. In Section 5, we show how to generate

multiple frames of data from a simulated dynamic scene situation. An algorithm for image reconstruction from multiple frames of data obtained from a dynamic scene is also described and the simulation results are illustrated.

**2. The method of projection onto convex sets**

Youla and Webb [5] proposed a method based on POCS for image reconstruction. The advantage of POCS method is that it enables any number of a priori convex-type constraints to be incorporated in the reconstruction algorithm. We follow this approach for image reconstruction from sparse data. We briefly review the method of POCS here.

The method of POCS follows an approach to find a solution from a collection of convex sets. It tries to find a solution that satisfies constraints known a priori. The solution belongs to a set of all functions satisfying the initial data and satisfying the given constraints. Assume that all functions of interest are elements of the Hilbert space  $\mathcal{H}$ . Consider a closed convex set  $C$ ,  $C \subset \mathcal{H}$ . It is required to show that this projection of  $f \in \mathcal{H}$  onto  $C$  assigns  $f$  its nearest neighbor in  $C$ . We state a theorem without proof [5].

**THEOREM 1.** Let  $C$  denote any closed convex subset of  $\mathcal{H}$  and let  $f$  be any element of  $\mathcal{H}$ . Then there exists a unique  $\tilde{f} \in C$  such that

$$\inf_{x \in C} \|f - x\| = \|f - \tilde{f}\|, \tag{2}$$

where  $\|\cdot\|$  is the norm. This clearly states that  $\tilde{f}$  is the element in  $C$  closest to  $f$  in the specified norm.

In this method, the unknown signal  $f$  is assumed to lie in the Hilbert space  $\mathcal{H}$ . In image reconstruction, every known property of the original image restricts it to lie in a closed convex subset of  $\mathcal{H}$ . In general  $m$  such properties will generate  $m$  well-defined closed convex sets,  $C_i$ ,  $i = 1, 2, \dots, m$ , and

$$\tilde{f} \in C_0 = \bigcap_{i=1}^m C_i. \tag{3}$$

It is required to find a point in the intersection, i.e., an image that lies in  $C_0$  as shown in Figure 1. The intersection set is also closed and convex, and any solution in the set is acceptable. If  $C_0$  has only one point, then the solution is unique; if  $C_0$  is empty, then there is no solution. But usually, when the sparse data is used,  $C_0$  contains many solutions. It is shown in Figure 1 how a solution can be obtained by projecting the initial estimate onto the convex sets. It is also shown geometrically that the final solution depends on the initial estimate. Any image in the restricted solution set will satisfy all the constraints and therefore represents a solution to the problem.

Let us denote the projection operators onto  $C_0$  and  $C_i$  by  $P_0$  and  $P_i$ , respectively. If  $C_0$  is not empty, then every fixed point of  $P_0$  is a fixed point of  $P_i$ . A fixed point is

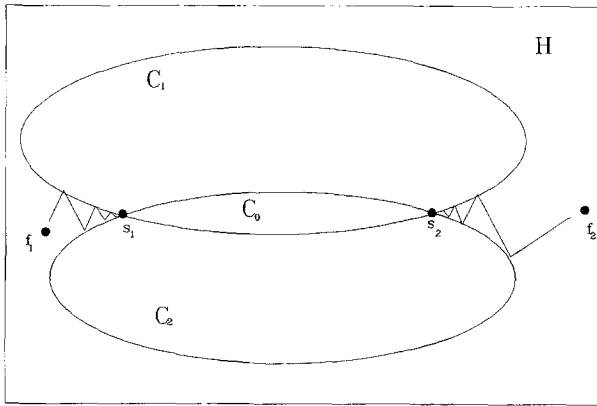


Figure 1. Projections onto two convex sets,  $C_1$  and  $C_2$ .  $C_0 = C_1 \cap C_2$ . Note that the solutions  $s_1$  and  $s_2$  obtained from two different initial estimates  $f_1$  and  $f_2$  are different but  $s_1, s_2 \in C_0$ .

obtained when the projection of a point onto a convex set no longer results in a new point, i.e.,  $P_0 \tilde{f} = \tilde{f}$ . If the projection operator  $P_0$  onto  $C_0$  is known, then the problem is solved. However projecting onto  $C_0$  is usually complex. Therefore the solution is obtained by the following iterative relation:

$$\tilde{f}^{k+1} = P_m P_{m-1} P_{m-2} \cdots P_1 f^k, \quad k = 0, 1, 2, \dots, \quad (4)$$

where  $f^0 \in \mathcal{F}$  is the initial image. In order to speed up the convergence, the projection operator is relaxed as shown in (6). Then (4) can be generalized as

$$\tilde{f}^{k+1} = T f^k, \quad k = 0, 1, 2, \dots, \quad (5)$$

where  $T (= T_m T_{m-1} T_{m-2} \cdots T_1)$  is a composite operator composed of relaxed parameters  $T_i$ , where

$$T_i = I + \beta_i (P_i - I), \quad i = 1, 2, 3, \dots, m, \quad (6)$$

where  $\beta_i$ 's are the relaxation parameters that control the rate of convergence,  $P_i$ 's are the projection operators, and  $I$  is the identity operator. The value of each relaxation parameter  $\beta$  is arbitrarily set between 0 and 2. This relaxation extends the projection beyond the contours. The advantage of this iteration is that the  $\beta_i$ 's can be adjusted for rapid convergence. If  $\beta_i$  is set to unity, then (5) reduces to (4). It is shown that  $T_i$ 's are generally not projectors but have the same fixed points as the  $P_i$ 's and every fixed point of  $T_i$  is a feasible solution, i.e., a point in the intersection of the closed convex sets as shown in Figure 1. The final solution depends on the initial guess. Any solution in the intersection is acceptable and is consistent with the a priori constraint. In the following sections, we show that this method can be adopted to reconstruct good-quality images from sparse data.

### 3. Sensor array imaging

In this section we briefly describe the theory of imaging. An object is illuminated by a plane wave, and the reflected wave pattern is captured on the receiver plane using a finite number of sensors. A typical SAI setup is shown in figure 2. The data obtained is usually a transformation of the original image. Therefore image reconstruction is done by computing the inverse transform of the received data. The relation between the object and the receiver field distribution is given by

$$g(x, y) = h(x, y) * f(x, y), \tag{7}$$

where  $f(x, y)$  is the image,  $g(x, y)$  is the receiver data,  $*$  is the convolution operator, and  $h(x, y)$  is the impulse response function given by [11]

$$h(x, y) = \frac{1}{j\lambda z} \exp(jk\sqrt{x^2 + y^2 + z^2}), \tag{8}$$

where  $z$  is the distance between the object and the receiver planes,  $k = 2\pi/\lambda$  is the wave number, and  $\lambda$  is the wavelength of the transmitted wave. Using the convolution theorem, the convolution in (7) can be written as

$$G(u, v) = H(u, v)F(u, v), \tag{9}$$

where  $G(u, v)$ ,  $F(u, v)$ , and  $H(u, v)$  are the 2-D Discrete Fourier transforms (DFT) of  $g(x, y)$ ,  $f(x, y)$ , and  $h(x, y)$ , respectively. The image  $f(x, y)$  is obtained by deconvolution. Multiplying both sides of (9) by  $H^{-1}(u, v)$  and taking inverse DFT, we obtain the image  $f(x, y)$ .

$$f(x, y) = \text{IDFT}[H^{-1}(u, v)G(u, v)], \tag{10}$$

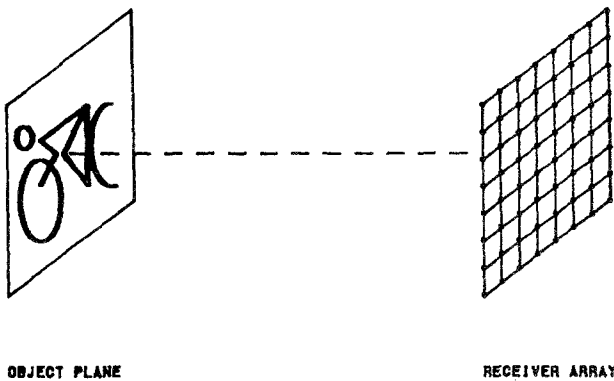


Figure 2. A typical sensor array imaging setup. The object and the receiver planes consist of the same number of points. The distance between the receiver and the object is  $z$  and  $\lambda$  is the wavelength of the transmitted wave. The reflected pattern is captured at the receiver plane.

where  $H^{-1}(u, v)$  is given by [11]

$$H^{-1}(u, v) = \begin{cases} \exp(jkz \sqrt{1 - (\lambda u)^2 - (\lambda v)^2}), & \text{for } 1 - (\lambda u)^2 - (\lambda v)^2 > 0, \\ 0, & \text{otherwise.} \end{cases} \quad (11)$$

If  $g(x, y)$  is known completely, a unique solution is obtained. However, in practice due to the limited number of sensors,  $g(x, y)$  is sparse. In such a case, a set of solutions is obtained. The solution set becomes larger as the sparsity of data increases. Our aim is to restrict the solution set and obtain a good-quality image from the sparse data. In Section 4, we show how the method of POCS can be used to restrict the solution set.

#### 4. Image reconstruction from sparse data

The SAI setup used for simulation studies consists of an object plane of  $128 \times 128$  points and a receiver plane of  $128 \times 128$  points. The original image is restricted to lie within  $64 \times 64$  grid. Throughout the studies the frequency used for imaging operation corresponds to a wavelength of 0.25 unit. The spacing between adjacent receiver points is fixed at 0.5 unit. The distance between the object and the receiver plane is kept at 2000 units. The receiver size in terms of the number of sensor elements is varied by selecting the points appropriately on the receiver array. We consider down sampling to generate sparse data in all our studies. We consider equally spaced sensors.

The field data is simulated for different array sizes. The field data for  $64 \times 64$ ,  $32 \times 32$ ,  $16 \times 16$ , and  $8 \times 8$  points on the receiver plane are collected. Finite support constraint is used as the a priori known information and is defined as

$$\tilde{f}_0(x, y) = \begin{cases} f_0(x, y), & \text{for } (x, y) \in \Gamma, \\ 0, & \text{otherwise,} \end{cases} \quad (12)$$

where  $f_0 \in \mathcal{H}$  and  $\Gamma$  is the support region. The initial image is assumed to lie in the Hilbert space. The field data corresponding to the initial estimate is generated. The calculated values are replaced by the measured values. Then the image is reconstructed using the new field data values. The solution is restricted by using the finite support constraint on the resulting solution. The detailed algorithm for reconstructing an image from sparse data is given below.

##### ALGORITHM 1. Image Reconstruction Using Single Frame of Data

1.  $i = 1$ . Let  $g_{k \times k}(x', y')$  be the measured field data where  $k \times k$  is the size of the receiver array. The field data is measured at points  $x' = x(128/k)$  and  $y' = y(128/k)$ , for  $x, y = 1, 2, \dots, 128$ .  $N =$  number of iterations. Let  $f_i(x, y)$  be the initial image.
2. Generate the field data corresponding to  $f_i(x, y)$ .  $g(x, y) = \text{IDFT}[H(u, v)F_i(u, v)]$ , where  $H(u, v)$  and  $F_i(u, v)$  are the DFT of  $h(x, y)$  and  $f_i(x, y)$  respectively. Since  $128 \times 128$  point DFT is used,  $g(x, y)$  has  $128 \times 128$  points.

3. Replace the calculated  $g(x, y)$  with the measured field data  $g_{k \times k}(x', y')$  at known points to obtain the new  $g(x, y)$ .
4. Reconstruct the image using deconvolution followed by the method of POCS.
  - a.  $G(u, v) = \text{DFT}[g(x, y)]$ .
  - b.  $f_i(x, y) = \text{IDFT}[H^{-1}(u, v)G(u, v)]$ . This image has  $128 \times 128$  points.
  - c.  $f_{i+1}(x, y) = I + \beta(Pf_i(x, y) - I)$ , where  $\beta = 0.8$ ,  $P$  is the projection onto the convex set formed by the finite support constraint, and  $I$  is the identity operator. Here,

$$Pf_i(x, y) = \begin{cases} f_i(x, y), & \text{for } (x, y) \in \Gamma, \\ 0, & \text{otherwise.} \end{cases}$$

5.  $i = i + 1$
6. Repeat step 2 through step 5 until  $i > N$ .

Figure 3 shows the original image with  $128 \times 128$  points. The image lies within  $64 \times 64$  points. Figures 4a–4d show the reconstructed image using  $64 \times 64$ ,  $32 \times 32$ ,  $16 \times 16$ , and  $8 \times 8$  points, respectively. The number of iterations in all the cases is 20. These figures clearly illustrate that the quality of the reconstructed image decreases as the size of the array decreases. The improvement in the quality of the image would be marginal even if the number of iterations are increased as illustrated in figure 5. Figures 5a–5d represent reconstructed images using  $32 \times 32$  points on the receiver plane after 10, 20, 50, and 100 iterations, respectively. The quantitative improvement in the reconstructed image is indicated using the signal-to-noise ratio (SNR) parameter.

$$SNR = 10 \log_{10} \left( \frac{\text{variance of the signal}}{\text{variance of the noise}} \right) \tag{13}$$

The plot in figure 6 shows that SNR improves up to about 20 iterations. The quality of the image does not improve significantly beyond about 20 iterations. This shows clearly that the quality of the image cannot be improved beyond certain limits. Additional information is required for obtaining a good-quality image. In the next section, we show how to collect additional measurements and show how to incorporate them to reconstruct images of good quality.



Figure 3. Original image ( $128 \times 128$ ) used for simulation studies. In this figure only the region of the image is shown.



*Figure 4.* Effect of poor sampling of the receiver data on the reconstructed image. The complete receiver data contains  $128 \times 128$  points. The figure shows the reconstructed images using different sampling rates. The unknown samples are set to zero. The figure shows the reconstructed image using (a)  $64 \times 64$  points on the receiver plane, (b)  $32 \times 32$  points on the receiver plane, (c)  $16 \times 16$  points on the receiver plane, (d)  $8 \times 8$  points on the receiver plane. In all cases only one frame of data is used for reconstruction, and finite support constraint is used as the a priori knowledge. Note the degradation when the number of sampling points decreases.



*Figure 5.* Effect of increased number of iteration on the reconstructed images. Only one frame of data obtained using  $32 \times 32$  points on the receiver plane is used for image reconstruction. The figure shows the reconstructed image after (a) 10 iterations, (b) 20 iterations, (c) 50 iterations, (d) 100 iterations. In all cases finite support constraint is used as the a priori knowledge.

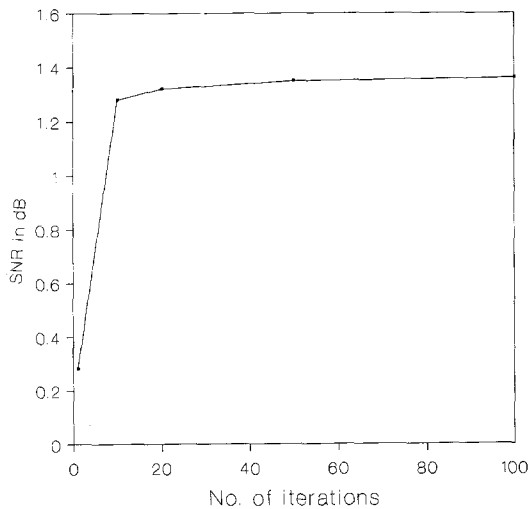


*Figure 6.* The quantitative improvement in the reconstructed images corresponding to Figure 5. The figure shows the SNRs of the reconstructed image versus the number of iterations used in the reconstruction. Note that there is only a very minimal improvement in the SNR after 20 iterations.

## 5. Image reconstruction from multiple frames of data

Additional field data can be obtained by several ways, such as by varying the frequency of the incident wave, object-receiver distance, etc. It had shown that high-resolution images can be reconstructed from multiple frames of sparse data [6–8]. Here we explore the possibility of using multiple frames of data obtained from a dynamic scene situation. In a practical imaging setup one would obtain multiple frames of data naturally when (i) the object is moving while the sensor array is stationary, (ii) the sensor array is moving while the object is stationary, and (iii) both the object and the sensor array are moving.

In our approach, the data collection is simulated for the case of a moving object, while the sensor array remains stationary. Let  $f(x, y)$  be the image with no background, and  $f_k(x, y)$ ,  $k = 1, 2, 3, \dots, M$  be the spatially shifted versions of  $f(x, y)$ . Then

$$f_k(x, y) = f(x + \delta x_k, y + \delta y_k), \quad (14)$$

where  $\delta x_k$  and  $\delta y_k$  are known shifts of  $f(x, y)$  along  $x$  and  $y$  coordinates, respectively.

Table 1 gives a set of arbitrarily chosen shift values. Figure 7a is the reference image. Each image in the sequence (Figures 7b–7j) is generated based on the shift information given in Table 1. Each pair of shift values in Table 1 represents shift values of the  $(n + 1)$ th image with respect to the  $n$ th image. Multiple frames of data (in this case 10) are simulated using  $32 \times 32$  points and  $16 \times 16$  points on the receiver plane for all the images shown in figure 7.

In the first experiment, we have used the multiple frames of data obtained using a  $32 \times 32$  receiver array. The first image in the sequence is reconstructed using Algorithm 1. The second image in the sequence is obtained by shifting the reconstructed image using the shift information given in Table 1. The field data corresponding transformed image is generated. The field data corresponding to the second frame is available for  $32 \times 32$  points. The calculated values are replaced by these known values. Then the second image is reconstructed using the new field data values. The detailed algorithm is given below. As more frames of data are included, the quality of the reconstructed image improves. This process is continued until all the frames of sparse data are used for reconstruction.

Table 1. Shift values used in the image reconstruction algorithm.

Frame number	Shift with respect to the previous frame
1	(Reference frame) 0,0
2	1,1
3	1,0
4	1,1
5	1,1
6	1,0
7	1,2
8	1,2
9	1,0
10	0,1

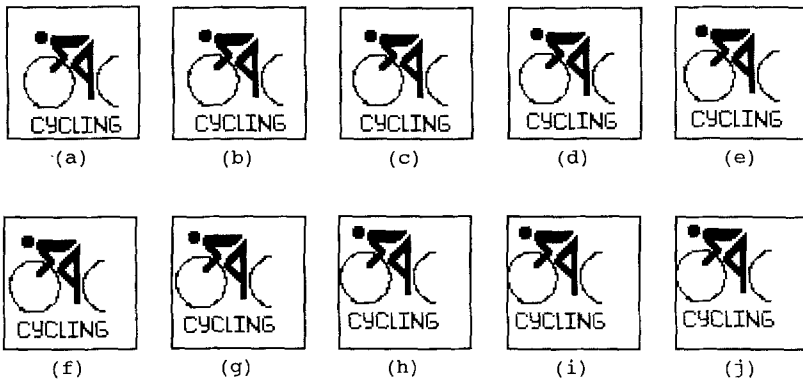


Figure 7. Simulated sequence of images ( $128 \times 128$  points) obtained from a dynamic scene situation. Figure 7a is used as the reference image. The images in Figures 7b-7j are obtained using the shift values given in Table 1. In this figure only the region of the image is shown.

ALGORITHM 2. High-Resolution Reconstruction from Multiple Frames of Data

1.  $M$  = total number of frames.  $i = 1$ . Let  $g_{k \times k}^i(x', y')$  be the measured field data of the  $i$ th frame where  $k \times k$  is the size of the receiver array. The field data is measured at points  $x' = x(128/k)$  and  $y' = y(128/k)$ , for  $x, y = 1, 2, \dots, 128$ . Let  $f^i(x, y)$  be the initial image.
2. Generate the field data corresponding to the  $i$ th frame  $f^i(x, y)$ .  $g^i(x, y) = \text{IDFT}[H(u, v) F^i(u, v)]$ , where  $H(u, v)$  and  $F^i(u, v)$  are the DFT of  $h(x, y)$  and  $f^i(x, y)$ , respectively. Since  $128 \times 128$  DFT is used,  $g^i(x, y)$  has  $128 \times 128$  points.
3. Replace the calculated field data  $g^i(x, y)$  with measured field data  $g_{k \times k}^i(x', y')$ .
4. Reconstruct the image using deconvolution followed by the method of POCS.
  - a.  $G^i(u, v) = \text{DFT}[g^i(x, y)]$
  - b.  $f^i(x, y) = \text{IDFT}[H^{-1}(u, v)G^i(u, v)]$ . This image has  $128 \times 128$  points.
  - c.  $\tilde{f}^i(x, y) = I + \beta(Pf^i(x, y) - I)$ , where  $\beta = 0.8$ ,  $P$  is the projection onto the convex set formed by the finite support constraint, and  $I$  is the identity operator. Here,

$$Pf^i(x, y) = \begin{cases} f^i(x, y), & \text{for } (x, y) \in \Gamma, \\ 0, & \text{otherwise.} \end{cases}$$

5. Using the shift information given in Table 1, transform the image and obtain the  $(i + 1)$ th image.  $f^{i+1}(x, y) = \tilde{f}^i(x + \delta x, y + \delta y)$ , where  $\delta x$  and  $\delta y$  are known shifts of  $\tilde{f}^i(x, y)$  along  $x$  and  $y$  coordinates, respectively.
6.  $i = i + 1$ .
7. Repeat step 2 through step 6 until  $i = M$ .

Figures 8b-8e represent the reconstruction of the fourth, sixth, eighth, and tenth images of the original sequence (figures 7b, 7d, 7f, 7g, and 7j), respectively. From the images

in Figure 8, it is clear that images with better resolution can be obtained when additional frames of the receiver data are used. A graph showing the improvement in image reconstruction in terms of SNR is shown in Figure 9. It is shown clearly in the plot (Figure 9) that the SNR increases as multiple frames of data are used in the image reconstruction. Figure 9 shows clearly the quantitative improvement in image. Note in Figure 8e that even the letters (CYCLING) are visible in the reconstructed image.

In the second simulation study, we have used  $16 \times 16$  points on the receiver array to collect the data. The reconstruction is done as before. Figures 10a–10e represent the reconstruction of the second, fourth, sixth, eighth, and tenth images of the original sequence (Figures 7b, 7d, 7f, 7g, and 7j), respectively. As the number of frames increases, the SNR values increases (Figure 11). This also indicates a quantitative improvement in the quality of the image.

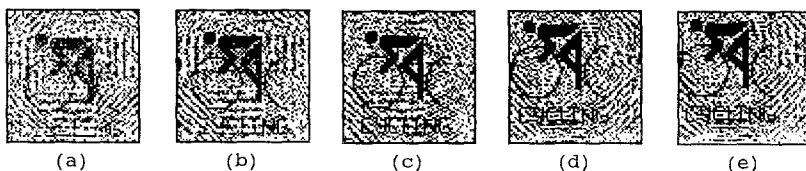


Figure 8. Images reconstruction using multiple frames of data obtained from a simulated dynamic scene situation. Multiple frames of data are collected for every image shown in Figure 7, using only  $32 \times 32$  points on the receiver plane. Finite support constraint is used in the reconstruction algorithm as a priori information. The figure shows the image reconstructed by combining (a) the first and the second frames of data, (b) the first four frames of data, (c) the first six frames of data, (d) the first eight frames of data, (e) all ten frames of data.

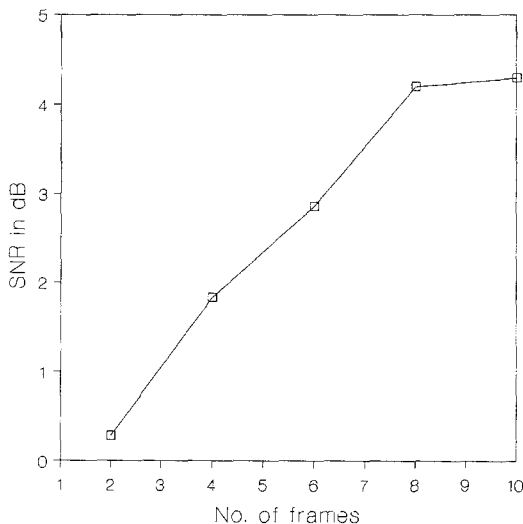
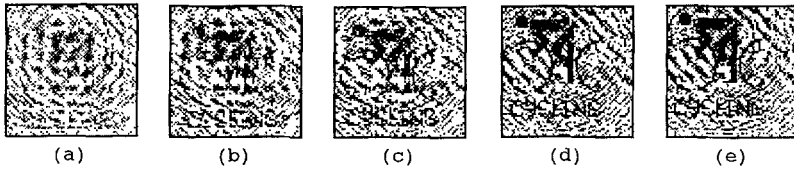
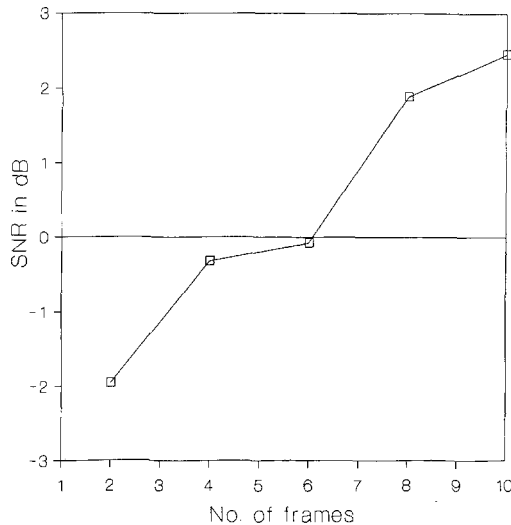


Figure 9. The quantitative improvement in the reconstructed images corresponding to Figure 8. Here SNRs of the reconstructed images versus the number of frames of data used in the reconstruction are shown in the plot. Note the increase in the SNR as additional frames of data are combined in the reconstruction algorithm.



*Figure 10.* Images reconstruction using multiple frames of data obtained from a simulated dynamic scene situation. Multiple frames of data are collected for every image shown in Figure 7, using  $16 \times 16$  points on the receiver plane. Finite support constraint is used in the reconstruction algorithm as a priori information. The figure shows the image reconstructed by combining (a) the first and second frames of data, (b) the first four frames of data, (c) the first six frames of data, (d) the first eight frames of data, (e) all ten frames of data.



*Figure 11.* The quantitative improvement in the reconstructed images corresponding to Figure 10. Here SNRs of the reconstructed images versus the number of frames of data used in the reconstruction are shown in the plot. Note the increase in the SNR as additional frames of data are combined in the reconstruction algorithm.

## 6. Conclusions

In this paper, we have proposed a method for solving an ill-posed problem that arises due to sparse data. The method of POCS is used to reduce the solution set by making use of the finite support constraint as the a priori information. Multiple frames of sparse data are used to improve the quality of the reconstructed image. It is obvious from our studies that the image quality improves as multiple frames of data are combined in the reconstruction algorithm as shown by the increasing SNR values in Figures 9 and 11. It is also shown that sparsity of data can be overcome by making use of the multiple frames of data. However, this method assumes that the motion parameters are known a priori. We are currently addressing the issue of estimating the motion parameters from poorly resolved images.

## Acknowledgments

The authors would like to thank the Department of Electronics (DoE), Government of India, for supporting this research activity at the Indian Institute of Technology, Madras. The authors would also like to thank the reviewers for their valuable comments and suggestions.

## References

1. M. Bertero, T.A. Poggio, and V. Torre, "Ill-Posed Problems in Early Vision," *Proc. IEEE*, vol. 76, 1988, pp. 917–935.
2. J. Biemond, R.L. Lagendijk, and R.M. Mersereau, "Iterative Methods in Image Deblurring," *Proc. IEEE*, vol. 78, 1990, pp. 856–883.
3. G. Demoment, "Image Reconstruction and Restoration: Overview of Common Estimation Structures and Problems," *IEEE Trans. Acoustic, Speech Signal Process.*, vol. ASSP-37, no. 12, 1989.
4. A.N. Tikhonov and A.V. Goncharsky, *Applications of Ill-Posed Problems in Natural Sciences*, Moscow: Mir, 1987.
5. D.C. Youla and H. Webb, "Image Restoration by the Method of Projections onto Convex Sets," *IEEE Trans. Med. Imaging Syst.*, vol. MI-1, no. 2, 1982.
6. B. Yegnanarayana, C.P. Mariadossu, and P. Saini, "Signal Reconstruction from Partial Data for Sensor Array Imaging Applications," *Signal Process.*, vol. SP-19, no. 2, 1990, pp. 139–149.
7. C.P. Mariadossu, "Solutions to Some Ill-Posed Problems in Sensor Array Imaging," Ph.D. Dissertation, Dept. Computer Science and Engineering, Indian Institute of Technology, Madras, India, 1990.
8. B. Yegnanarayana, R. Ramaseshan, and A. Ravichandran, "Image Reconstruction from Multiple Frames of Data," in Indo-US Workshop on Spectrum Analysis in One and Two Dimensions, New Delhi, India, 1989, pp. 367–382.
9. S.P. Kim, S.K. Bose, and H.M. Valenzuela, "Recursive Reconstruction of High Resolution Image from Noisy Undersampled Multiframe," *IEEE Trans. Acoustic, Speech Signal Process.*, vol. ASSP-37, no. 6, 1990, pp. 1013–1027.
10. B. Yegnanarayana, R. Ramaseshan, and A. Ravichandran, "Improving Resolution of Sensor Array Using Multiple Frames of Data," in 19th Int. Symp. Acoustical Imaging, Bochum, Germany, 1991.
11. J.L. Sutton, "Underwater Acoustic Imaging," *Proc. IEEE*, vol. 67, 1979, pp. 554–565.